RNA (2002), *8*:83–96. Cambridge University Press. Printed in the USA.

DOI: 10.1017.S1355838201013863

NMR structure and dynamics of the RNA-binding site for the histone mRNA stem-loop binding protein

ERIC S. DEJONG,[1] WILLIAM F. MARZLUFF,[2] and EDWARD P. NIKONOWICZ[1]

[1]Department of Biochemistry and Cell Biology, Rice University, Houston, Texas 77251-1892, USA
[2]Program in Molecular Biology and Biotechnology, Department of Biochemistry and Biophysics, University of North Carolina, Chapel Hill, North Carolina 27599, USA

ABSTRACT

The 3′ end of replication-dependent histone mRNAs terminate in a conserved sequence containing a stem-loop. This 26-nt sequence is the binding site for a protein, stem-loop binding protein (SLBP), that is involved in multiple aspects of histone mRNA metabolism and regulation. We have determined the structure of the 26-nt sequence by multidimensional NMR spectroscopy. There is a 16-nt stem-loop motif, with a conserved 6-bp stem and a 4-nt loop. The loop is closed by a conserved U•A base pair that terminates the canonical A-form stem. The pyrimidine-rich 4-nt loop, UUUC, is well organized with the three uridines stacking on the helix, and the fourth base extending across the major groove into the solvent. The flanking nucleotides at the base of the hairpin stem do not assume a unique conformation, despite the fact that the 5′ flanking nucleotides are a critical component of the SLBP binding site.

Keywords: 3′ processing; hairpin; heteronuclear; multidimensional; pre-mRNA; tetraloop

INTRODUCTION

Maturation of mRNA in metazoans involves multiple processing steps of the pre-mRNA transcript, including excision of introns and the addition of a poly(A) tail to the 3′ end. However, the replication-dependent histone mRNAs are unique, as the histone genes lack introns and the mature histone mRNAs terminate with a stem-loop (hairpin) secondary structure rather than poly(A) tails (Birnstiel et al., 1985; Marzluff, 1992; Dominski & Marzluff, 1999). Processing of the histone pre-mRNA transcript involves a single endonucleolytic cleavage event 3′ to the stem-loop (Gick et al., 1986). Two defined *trans*-acting components participate in the processing reaction—a protein that specifically binds the stem-loop (Wang et al., 1996; Martin et al., 1997) and the U7 snRNP that interacts with a purine-rich element located downstream of the cleavage site (Mowry & Steitz, 1987; Soldati & Schümperli, 1988). There are likely to be additional factors required for processing, including a heat-labile factor that has not been well characterized (Gick et al., 1987; Lüscher & Schümperli, 1987). Following 3′-end processing, the histone mRNA is rapidly transported to the cytoplasm. The 3′ terminal hairpin is necessary for efficient pre-mRNA processing (Pandey et al., 1994) and mRNA export (Eckner et al., 1991; Williams et al., 1994) and is essential for regulation of the histone mRNA half-life (Pandey & Marzluff, 1987).

The primary structure of the 3′ end of histone mRNAs is highly conserved and serves as the principle recognition element of the stem-loop binding protein (SLBP). The minimal recognition site for the SLBP is 26 nt (Williams & Marzluff, 1995) and it is predicted to form a 6-bp stem capped by a 4-nt pyrimidine-rich loop. The 5′ end of the stem is flanked by A/C-rich sequences essential for SLBP binding (Williams & Marzluff, 1995) and the 3′ end of the stem is followed by a consensus element ACCCA or ACCA, which is the cleavage target and plays a minor role in SLBP binding (Furger et al., 1998). High affinity binding of the SLBP to the hairpin depends on nucleotide identity within the loop, the stem, and the immediate 5′ and 3′ flanking sequences. The first and third residues of the loop are uridine nucleo-

Reprint requests to: Edward P. Nikonowicz, Department of Biochemistry and Cell Biology, Rice University, Houston, Texas 77251-1892, USA; e-mail: edn@bioc.rice.edu.

Abbreviations: DQF-COSY: double quantum filtered correlated spectroscopy; HetCor: heteronuclear correlation; HMQC: heteronuclear multiple quantum coherence; HSQC: heteronuclear single quantum coherence; NH: imino; NH_2: amino; NMR: nuclear magnetic resonance; NOE: nuclear Overhauser effect; NOESY: NOE spectroscopy; NTP: nucleoside triphosphate; rMD: restrained molecular dynamics; rmsd: root mean square deviation; SLBP: stem-loop binding protein.

tides in all metazoans except for *Caenorhabditis elegans*, which has a C in the first position (Roberts et al., 1989; Marzluff, 1992). The second position is predominantly occupied by uridine. U, C, and A are found in the fourth position but never G.

The sequence of the stem is critical for RNA binding (Battle & Doudna, 2001; Williams & Marzluff, 1995). The consensus stem sequence consists of two G•C base pairs, followed by three Y-R base pairs that generally contain at least two C•G base pairs, and an invariant U•A base pair at the top of the stem. Mutagenesis studies showed that the second G•C base pair is particularly critical for SLBP binding (Battle & Doudna, 2001). Although the proposed loop is composed of 4 nt, it is not a member of the unusually stable family of 4-nt loops known as tetraloops. Indeed, the most similar tetraloop family, UNCG, is excluded by the invariant absence of guanine at position four. The 5′-U and 3′-A nucleotides that close the loop are invariant. Similar sequence motifs in which apposing U and A nucleotides flank a loop but do not base pair, such as stem-loop IIa of yeast U2 snRNA, suggest that the histone 3′ mRNA hairpin might alternatively have a stem of 5 bp and a loop of 6 nt. The reduced length of the stem and the conserved adenine nucleotides that flank the 5′ side of the hairpin that could pair with nucleotides in the loop suggest the possibility that the SLBP recognition element contains a pseudoknot.

Although the SLBP is believed to recognize a unique tertiary structure adopted by the 3′ element, cleavage of the phosphate backbone within the loop does not impair the ability of the RNA to bind the SLBP (Williams & Marzluff, 1995). This result coupled with the finding that critical determinants for binding reside in the stem sequence and the flanking sequence 5′ of the stem, suggest that multiple contacts exist between the SLBP and the histone mRNA 3′ end.

We have used heteronuclear nuclear magnetic resonance (NMR) spectroscopy to determine the solution structure and dynamics of the 3′ end of histone mRNA in a 28-nt RNA molecule that contains the 26 nt necessary for SLBP binding. Our results confirm the predicted secondary structure of a 6-bp stem capped by a 4-nt loop. The nucleotides flanking the 5′ and 3′ ends of the stem are largely disordered and presumably only become ordered after forming specific contacts with SLBP. The implications of the stem-loop structure for SLBP binding are discussed.

RESULTS

Two RNA molecules (Fig. 1) were used in our structural study of the histone mRNA 3′ binding site for the SLBP. SL_{28} comprises the wild-type binding site for mammalian SLBP. The proposed secondary structure is a stem-loop flanked on either side by short single-stranded RNA sequences. Several conditions were tested to assess the effects of counterions and pH. K^+ is the physiologically relevant counterion within the cell and yielded the best quality spectrum. Na^+ and Mg^{2+} cause slight broadening and small chemical shift changes of the imino (NH) resonances, but do not lead to the appearance of new peaks. The reduction of pH from 6.8 to 5.7 also results in slight broadening and weakening of the NH resonances.

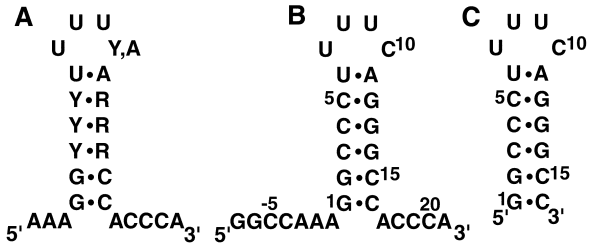

FIGURE 1. Sequence and proposed secondary structures of (**A**) the conserved RNA binding site for the histone SLBP, (**B**) the 28-nt RNA molecule, SL_{28}, used in this study, and (**C**) the 16-nt RNA molecule, SL_{16}, also used in this study. Residues in SL_{28} are numbered relative to the 5′ terminal G of the proposed stem-loop.

Chemical shift assignments

The sequence-specific assignment of SL_{28} is hindered by resonance overlap of 1′ and pyrimidine base resonances. Approximately 65% of the ^1H and ^{13}C resonances can be unambiguously assigned using standard heteronuclear methodologies. Nonetheless, the NH spectrum with 5 G NH resonances characteristic of G•C base pairs and 1 U NH resonance characteristic of an A•U base pair clearly indicate that SL_{28} forms a hairpin (Fig. 2). A pseudoknot conformation with the flanking As paired with the loop Us should produce additional downfield shifted U NH resonances. Although the NH spectrum largely establishes the global fold of SL_{28}, poor resolution of several nonexchangeable resonances from the loop nucleotides impair a high resolution structure determination of the RNA. To facilitate assignment of SL_{28} and improve the accuracy of the three-dimensional structure, SL_{16}, the RNA hairpin without the flanking sequences, was studied (Fig. 1).

The exchangeable NH and amino (NH_2) resonances were assigned using two-dimensional nuclear Overhauser effect (NOE) spectroscopy (NOESY) and two-dimensional ^{15}N-edited NOESY experiments. Briefly, the NH resonance of the U•A base pair was first identified by the characteristic ^{15}N chemical shift of its NH resonance. The remaining NH resonances were assigned using the weaker NOE connectivities between NH proton resonances of neighboring base pairs. These connectivities are continuous in the helix from G_2 to G_{11}. The cytidine NH_2 resonances were assigned using the strong intra-base-pair C NH_2 to G NH NOE cross-peaks. Independent confirmation of the resonance as-

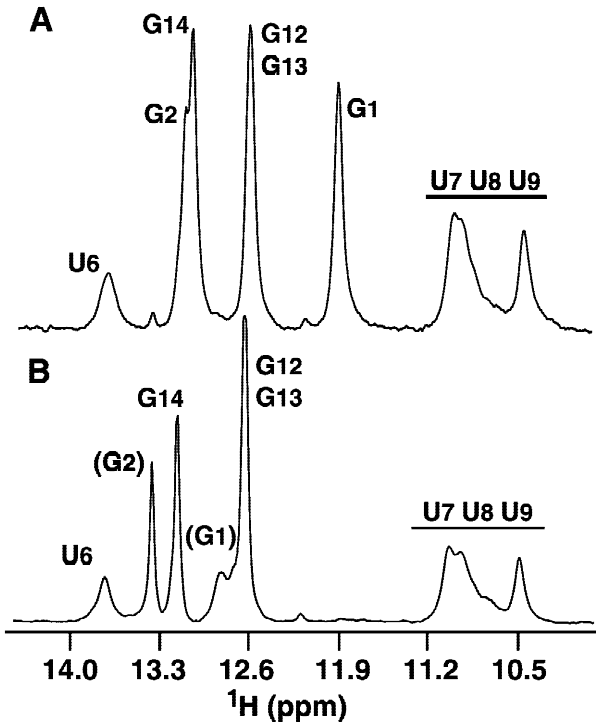

FIGURE 2. One-dimensional NH ^{1}H spectra of SL_{28} (**A**) and SL_{16} (**B**) RNA molecules. The flanking regions of SL_{28} cause upfield and downfield shifts of the G_1 and G_2 resonances, respectively, relative to those of SL_{16}. The chemical shifts of the remaining NH resonances, including those corresponding to the loop uridine nucleotides, are the same and demonstrate that SL_{16} and SL_{28} have equivalent secondary structures. The identical peak pattern of the loop uridine resonances also confirms that the adenine bases of the 5′ flanking sequence do not interact with the loop to form a pseudoknot.

signments was provided by strong cytidine intrabase NH_2 to H5 NOE cross-peaks in G•C base pairs. The NH proton resonances of U_7, U_8, and U_9 are resolved but broad with chemical shifts 10.5–11.0 ppm, a region of the NH proton spectrum characteristic of unpaired uridine nucleotides. The NH_2 resonances of G_1, G_2, and A_{11} were not observed and could not be assigned. All other exchangeable proton and protonated nitrogen resonances were assigned. Although divalent metal ions are not required for SLBP binding or 3′ end processing, a two-dimensional ^{15}N-^{1}H heteronuclear multiple quantum coherence (HMQC) spectrum was collected for SL_{16} after addition of 10 mM Mg^{2+}. No chemical shift changes are observed and only the U_6 NH resonance is slightly weakened. This suggests that Mg^{2+} may associate with the RNA loop and accelerate solvent exchange of the U_6 NH proton, but does not induce significant structural changes. This is consistent with the finding that binding of SLBP and histone pre-mRNA processing occur efficiently in 20 mM EDTA.

The nonexchangeable ^{1}H and ^{13}C resonances of SL_{16} (Fig. 1) were assigned using standard heteronuclear techniques (Pardi, 1995; Dieckmann & Feigon, 1996). Most of the base and ribose ^{1}H-^{13}C correlations are resolved and none of the resonances have spectral characteristics indicative of intermediate exchange. All 16 ribose spin systems were identified using three-dimensional HCCH-COSY and three-dimensional HCCH-TOCSY experiments. Intraresidue base-to-sugar correlations were identified using two-dimensional ^{15}N-^{1}H HSQC experiments optimized to yield the multiple bond correlations H5-N1, H8-N9, and H1′-N1/N9 (Dieckmann & Feigon, 1996). All residues except C_3 and C_{16} yielded the desired base-ribose correlations.

Sequential assignments for the nonexchangeable resonances were made using three-dimensional ^{13}C-edited NOESY experiments to identify sequential H6/8-H1′ NOE connectivities (Pardi, 1995). The intraresidue ^{15}N-^{1}H base-to-sugar correlations permitted intraresidue cross-peaks to be distinguished from interresidue cross-peaks. The sequential H6/8-H1′ NOE connectivities are continuous through all 16 nt in the 180 ms NOESY spectrum. The H6/8-H2′ interresidue connectivities also are continuous through the hairpin except between C_{10} and A_{11}. This is consistent with disruption of the backbone introduced by the C2′-endo ribose ring conformation of C_{10}. Interestingly, i to i + 2 NOE cross-peaks from U_9 H1′ to A_{11} H8 and U_9 H6 to A_{11} H1′ were observed, suggesting exclusion of the C_{10} base from the loop.

All internucleotide ^{31}P resonances are dispersed between −3.4 and −4.6 ppm. All 15 ^{31}P resonances were able to be assigned using the H3′-P correlations from two-dimensional ^{31}P-^{1}H heteronuclear correlation (HetCor) spectra. Several P-H4′ and P-H5′/H5″ correlations also were present in the HetCor spectra. These assignments were later confirmed from a sequential walk in a two-dimensional ^{31}P-^{1}H hetero-TOCSY-NOESY experiment.

The secondary structure shared by SL_{28} and SL_{16} is evident through comparison of the NH ^{1}H spectra (Fig. 2). Except for the 5′ terminal residue of the hairpin G_1, the peaks in each spectrum have nearly identical chemical shifts, indicating that SL_{16} and SL_{28} have a common secondary structure. Importantly, the matching chemical shifts of the corresponding unpaired U NH resonances demonstrate that the loop uridines do not interact with nucleotides of the flanking sequences.

The nonexchangeable resonances of the SL_{28} RNA molecule were assigned using the same methods employed to assign SL_{16}, except that a pyrimidine-C5-deuterated molecule was used to help reduce overlap in NOESY spectra (Nikonowicz et al., 1998). All six adenine C2-H2 correlations are resolved and only A_{11} of SL_{28} has ^{1}H and ^{13}C chemical shifts that match the C2-H2 pair of A_{11} in SL_{16} (Fig. 4). Similarly, the A_{11} H2-N1/N3 cross-peaks of SL_{28} align with the A_{11} H2-N1/N3 correlations of SL_{16}, confirming the A_{11} chemical environments are equivalent in the two molecules (Fig. 3A). The chemical shifts of the base ^{1}H-^{13}C cor-

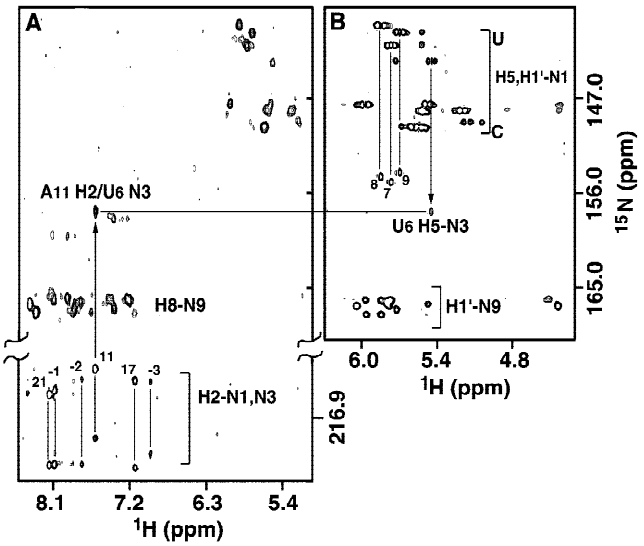

FIGURE 3. Base proton region of the HNN-COSY spectrum (**A**) and sugar proton region of the multiple-bond ^{15}N-^{1}H HSQC spectrum (**B**) of SL_{28}. The U_6 NH proton exchanges with solvent too rapidly to give rise to cross-peaks in the NOESY spectrum, preventing confirmation of the U_6-A_{11} base pair by conventional means. However, the U_6 H3-to-A_{11} N1 hydrogen-bond-mediated coupling of U_6 N3 to A_{11} N1 yields the A_{11} H2-U_6 N3 correlation (**A**). The six adenine H2-N1, N3 correlation pairs are connected in **A** and the four uridine H5-N1, N3 correlation pairs are connected in **B**.

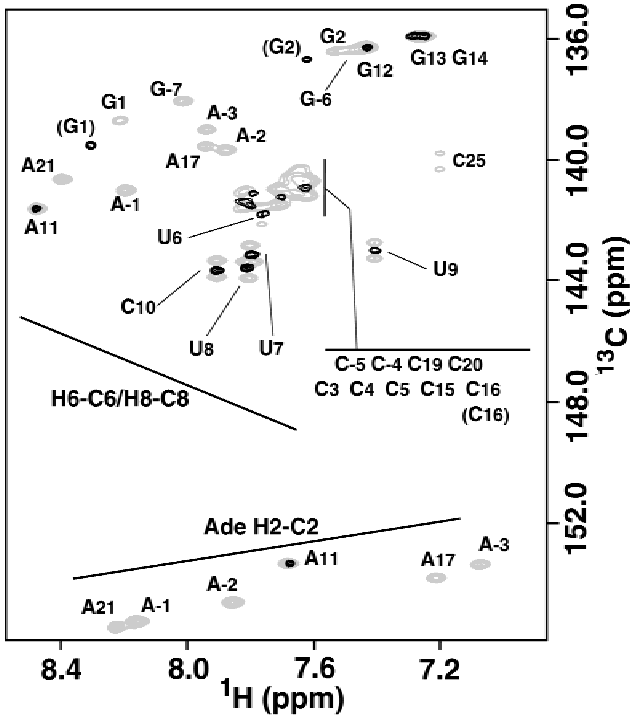

FIGURE 4. Overlay of base C6/8 and C2 regions of ^{13}C-^{1}H HSQC spectra of SL_{16} (black) and SL_{28} (gray) hairpins. Identifiers for cross-peaks from SL_{16} that are not degenerate with the corresponding cross-peaks of SL_{28} are enclosed in parentheses. The nonhelix cytidine resonances of SL_{28} lead to severe overlap of most of the cytidine C6H6 resonance pairs, including those in the stem. The spectrum of the SL_{16} hairpin reveals the positions of the stem cytidine base-6 resonances.

relations of residues within the 16-nt hairpin of SL_{28} are identical with those of SL_{16} (Fig. 4). The terminal G_1 residue is an exception due to the presence of the flanking sequences. Using the resonance assignments of the SL_{16} hairpin, it was possible to identify the corresponding ribose spin systems of SL_{28} from the three-dimensional ^{13}C-^{1}H HCCH-TOCSY spectrum. The ^{15}N-^{1}H multiple-bond correlated spectrum (Fig. 3B) yielded improved resolution of hairpin and flanking region base and ribose 1′ ^{1}H resonances and facilitated sequential resonance assignment of the SL_{28} RNA using the H6/8-H1′ region of the NOESY spectrum. The ^{1}H, ^{13}C, and ^{15}N chemical shifts are listed in the Appendix.

Structures of the SL_{16} and SL_{28} molecules

The structures of SL_{16} and SL_{28} were calculated using a restrained molecular dynamics routine starting from 40 structures with completely random backbone dihedral angles. The calculations for SL_{16} used a total of 296 conformationally restrictive distance constraints and 50 dihedral angle constraints (Table 1) to produce 12 converged structures (Fig. 5). For SL_{28}, 333 NOE-derived distance constraints and 66 dihedral angle constraints were used to produce 11 converged structures. The converged structures had an average of 11 distance constraint violations between 0.1 and 0.3 Å, randomly distributed throughout the hairpins. All converged structures violated no NOE constraints by more than 0.3 Å. The heavy atoms of the SL_{16} final converged structures superpose on the average structure with an average root mean square deviation (rmsd) of 1.25 Å. The heavy atoms of the 16 nt composing the hairpin of SL_{28} superpose with an average rmsd of 1.34 Å. The local precision of the hairpins is better, though, with the loop (U_6-A_{11}) and stem (G_2-U_6 and A_{11}-C_{15}) regions of SL_{28} having rmsds of 0.51 Å and 0.85 Å, respectively.

The conformations of SL_{16} and the central hairpin of SL_{28} differ only slightly near the helix terminus and are described together. The pyrimidine C5-deuterated SL_{16} RNA hairpin was important for extraction of loop region base–base and base–H1′ constraints due to resonance crowding in both ^{1}H and ^{13}C dimensions. Figure 6 summarizes the experimental distance constraints for the loop and upper stem. The abundance of distance constraints in the loop region (residues U_6-A_{11}) defines the conformation of these nucleotides very precisely (Fig. 5A; Table 1). Sequential NOEs between H5 and H6 protons from U_6 through U_8 indicate that U_7 and U_8 form a 5′ base stack. NOEs from U_9 H6 to A_{11} H2 and H8 and the near absence of interresidue NOEs involving the C_{10} base indicate the proximity of U_9 and A_{11} and the relative distal position of the C_{10} base.

TABLE 1. Summary of experimental distance and dihedral angle constraints and refinement statistics for SL_{16} and SL_{28}.

Constraint		SL_{16}	SL_{28}
NOE distance constraints			
Intraresidue[a]		87	110
Interresidue		135	189
Mean number per residue		16	11
NOE constraints by category			
Very strong	(0.0–3.0 Å)	6	7
Strong	(0.0–4.0 Å)	36	36
Medium	(0.0–5.0 Å)	91	113
Weak	(0.0–6.0 Å)	85	105
Very weak	(0.0–7.0 Å)	4	4
Base pair constraints			
Total		34	34
Dihedral angle constraints			
Ribose ring[b]		24	24
Backbone		55	55
Mean number per residue		4.9	2.8
Violations			
Average distance constraints > 0.3 Å[c]		0	0
Average dihedral constraints $> 0.5°$[d]		19	19
Rmsd from ideal geometry[e]			
Heavy atoms (Å)		1.45	7.63
Backbone atoms (Å)		1.52	7.70

[a]Only conformationally restrictive constraints are included.
[b]Three torsion angles within each ribose ring were used to constrain the ring to either the C2′-endo or C3′-endo conformation. The ring pucker of residues G_{-7} to A_{-1}, U_7, and A_{17} to A_{21} were not constrained.
[c]A distance violation of 0.3 Å corresponds to 5.0 kcal energy penalty.
[d]A dihedral angle violation of 0.5° corresponds to 0.05 kcal energy penalty.
[e]Calculated against the minimized average structure.

Unusual interresidue sugar-to-sugar and sugar-to-base NOEs also play a key role in defining the structure of the loop (Fig. 6). These include NOEs from U_6 H2′ to U_7 H1′, U_8 H1′ to U_9 H1′, C_{10} H5′/5″ to A_{11} H8, and U_9 H1′, H3′ to A_{11} H8. These NOEs indicate that the sugar rings and 3 of the 4 bases of the loop pack together tightly in an arrangement distinctly different from standard helices.

Several nucleotides in the loop have unusual sugar–phosphate backbone conformations. The large H1′–H2′ couplings of residues U_8, U_9, and C_{10} indicate that their ribose sugar rings have the C2′-endo conformation and the >5 Hz P–H′/H5″ coupling of residues U_8, U_9, and C_{10} exclude β from the standard trans conformation. H4′–H5′/H5″ couplings >5 Hz in the DQF-COSY spectrum indicate that residues U_7 to U_9 have nonstandard γ backbone angles. These angles were left unconstrained and occupy the *trans* and gauche$^-$ conformations, respectively, in all converged structures (Fig. 7). The ϵ torsion angles of U_9 and C_{10} adopt the gauche$^-$ conformation and lie outside the *trans* region typical of A- or B-form geometries. These angles appear to facilitate the turn of the phosphate backbones in the loop. A nonstandard *trans* conformation for the α and ζ backbone angles is predicted to cause a downfield shift of the corresponding ^{31}P resonance (Gorenstein, 1984). Because the ^{31}P resonances of SL_{28} all cluster at −4.0 ppm, it is unlikely any of these angles adopt the *trans* conformation. However, no α and ζ angles were constrained. Except for residues U_6 and A_{11}, which have gauche$^+$ α torsion angles, U_7 to C_{10} adopt the more common gauche$^-$ conformation. Similarly, the ζ torsion angles tend to have the gauche$^-$ conformation except for those of U_8 and U_9, which lie between gauche$^+$ and *trans*. However, none of the α or ζ torsion angles in the loops of the converged structures have a true *trans* conformation (Fig. 7).

A superposition of the loop regions from the 11 converged structures is shown in Figure 5A and the minimized average structure is shown in Figure 7A. The helical base stack continues up the 5′ side of the loop, with U_8 stacking on top of U_7, which in turn stacks on top of the U_6•A_{11} base pair. Residue U_9 stacks above A_{11} and is nearly coplanar with U_7. However, there is no evidence to support hydrogen-bond interactions between U_7 and U_9. Residue C_{10} does not participate in either the 5′ or 3′ base stack but instead its base points out into solution on the major groove side of the helix. The stacking of the loop nucleotides has the net effect of extending the helix by an additional base pair step.

The pattern of intra- and interresidue H6/8-H1′ and H6/8-H2′ NOEs in the stem region does not significantly differ from that expected of standard A-form geometry. Although the U_6 NH resonance has no NOEs that would permit the direct identification of a base pair partner, the U_6 NH nitrogen and hydrogen nuclei resonate in the downfield region of the spectrum characteristic of Watson–Crick A•U base pairs. The only possible cross-strand partner for U_6 is A_{11}. The J(N, N)-HNN-COSY spectrum (Hennig & Williamson, 2000) yields a U_6 N3 to A_{11} H2 cross-peak, confirming the presence of the U_6 NH3 to A_{11} N1 hydrogen bond and thus the integrity of the U_6•A_{11} base pair (Fig. 3). The bases of the terminal G_1•C_{16} and U_6•A_{11} base pairs have interresidue NOEs consistent with base–base stacking. The sugar and phosphate backbone torsion angles in the stem also lie within the limits of A-form RNA helices.

The 5′ and 3′ flanking regions are poorly constrained by the NOE and J-coupling data. The sparseness of constraints for these residues leads to an array of conformations. The spectral data indicate that the A-rich 5′ sequence does not interact with the U-rich loop. Further, there is no evidence to suggest the presence of cross-strand A$^+$•C interactions between pH 5.7 and 6.8. Although the nucleotides in these regions exhibit intra- and interresidue NOEs sufficient to provide sequential resonance assignments and to confirm that the glycosidic bonds of all flanking region nucleotides have the *anti* conformation, no interresidue base–base NOEs could be identified that would indicate the flanking residues adopt a base-stacked helical conformation.

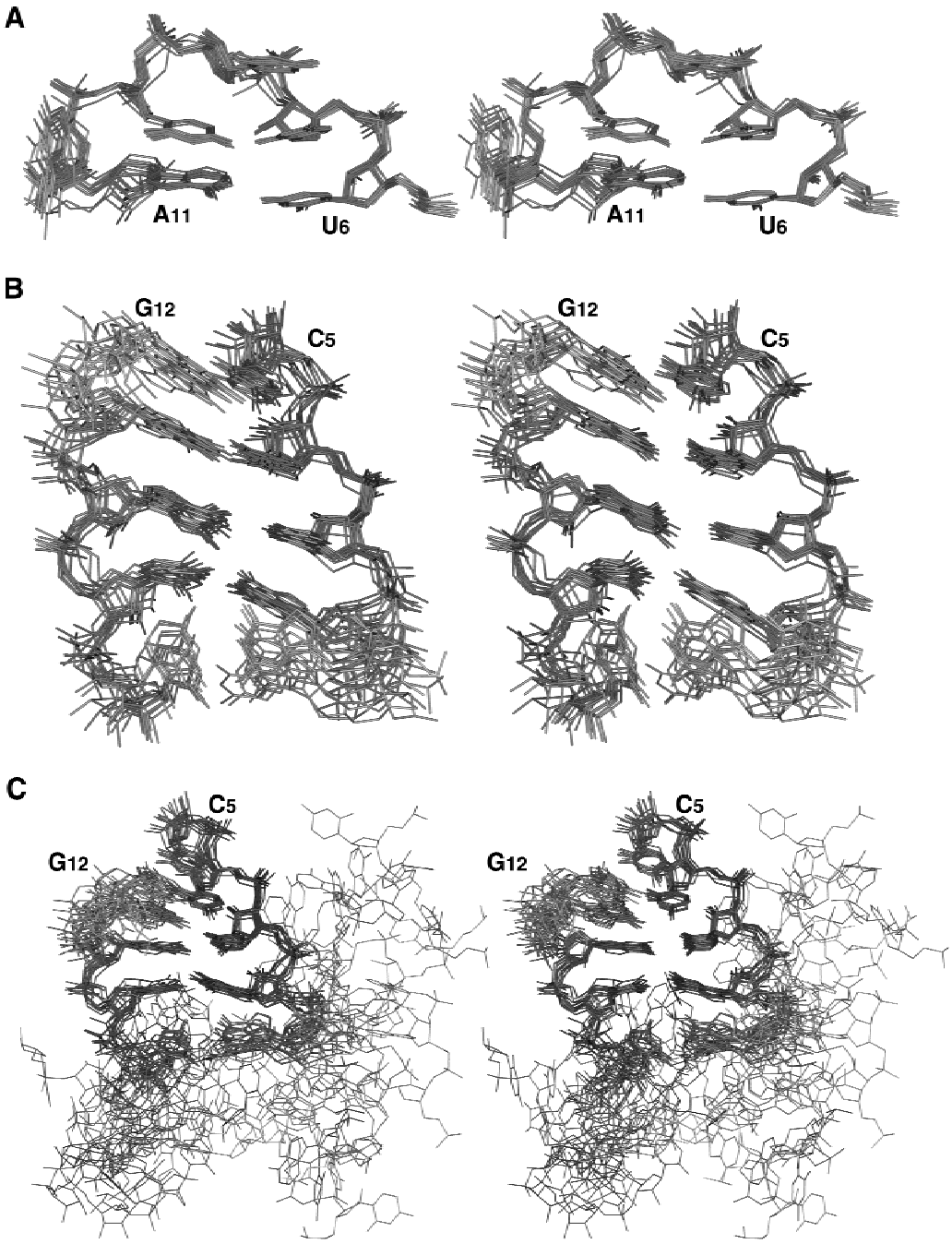

FIGURE 5. Stereoview of the local superposition of all 11 converged structures of SL_{28} for the loop (**A**), stem (**B**), and stem plus flanking regions (**C**). All views are into the major groove. The rmsds between the individual structures and the average structure are listed in Table 1. The loop and stem regions are generally well defined. The disorder of the flanking regions and of C_{10} are consistent with the dynamic character of these residues reflected in the relatively long $T_{1\rho}$ relaxation times. The calculations for the SL_{16} RNA hairpin yielded a similar distribution of converged structures.

^{13}C Relaxation measurements

The reorientation of a ^{13}C-^{1}H bond vector on the picosecond time scale can be assessed through its carbon $T_{1\rho}$ relaxation: The longer the relaxation time, the more mobile the ^{13}C-^{1}H pair (Yamazaki et al., 1994). The $T_{1\rho}$ relaxation times for the base C6 and C8 and ribose C1′ positions of SL_{16} are listed in Table 2. Cross-peak overlap in the SL_{28} spectrum permitted accurate measurement of the adenine C2 nuclei and only a few C8 nuclei and could not be used to assess the relative mobilities of stem and loop nucleotides. The C_{10} C6 nucleus has a relaxation time of 80 ms, whereas the U6, U9 and stem cytidine C6 nuclei have relaxation times of 46–55 ms. Loop nucleotides U_7 and U_8 have relaxation times intermediate between the stem residues and C_{10}.

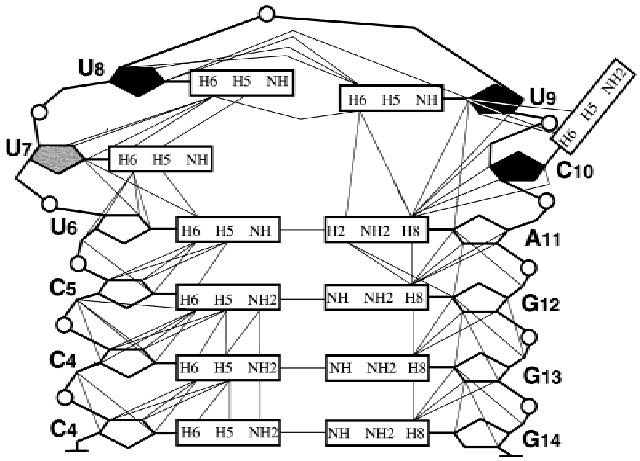

FIGURE 6. Schematic diagram summarizing several NOEs identified in the bulge and upper stem regions of the RNA hairpins. Ribose sugar conformations are indicated as C3′-endo (open), C2′-endo (filled), or mixed C3′/C2′-endo (gray).

A similar pattern is repeated for the C1′ nuclei. The flanking sequence C2 $T_{1\rho}$ values range from 24 to 80 ms with an average of 42 ms whereas the $T_{1\rho}$ value of A_{11} C2 is 26 ms. The increased mobilities of residue C_{10} and of the flanking residues indicated by their long relaxation times are consistent with a looped-out conformation of the cytidine base and little conformational rigidity among flanking nucleotides.

DISCUSSION

SLBP binds specifically to a 26-nt sequence that is present at the 3′ end of the replication-dependent histone mRNAs of all metazoans. It also binds to the histone pre-mRNA and this binding event is probably the initial step in histone pre-mRNA processing (Dominski & Marzluff, 1999; Dominski et al., 1999). Extensive mutagenesis of the 26-nt sequence has defined the pri-

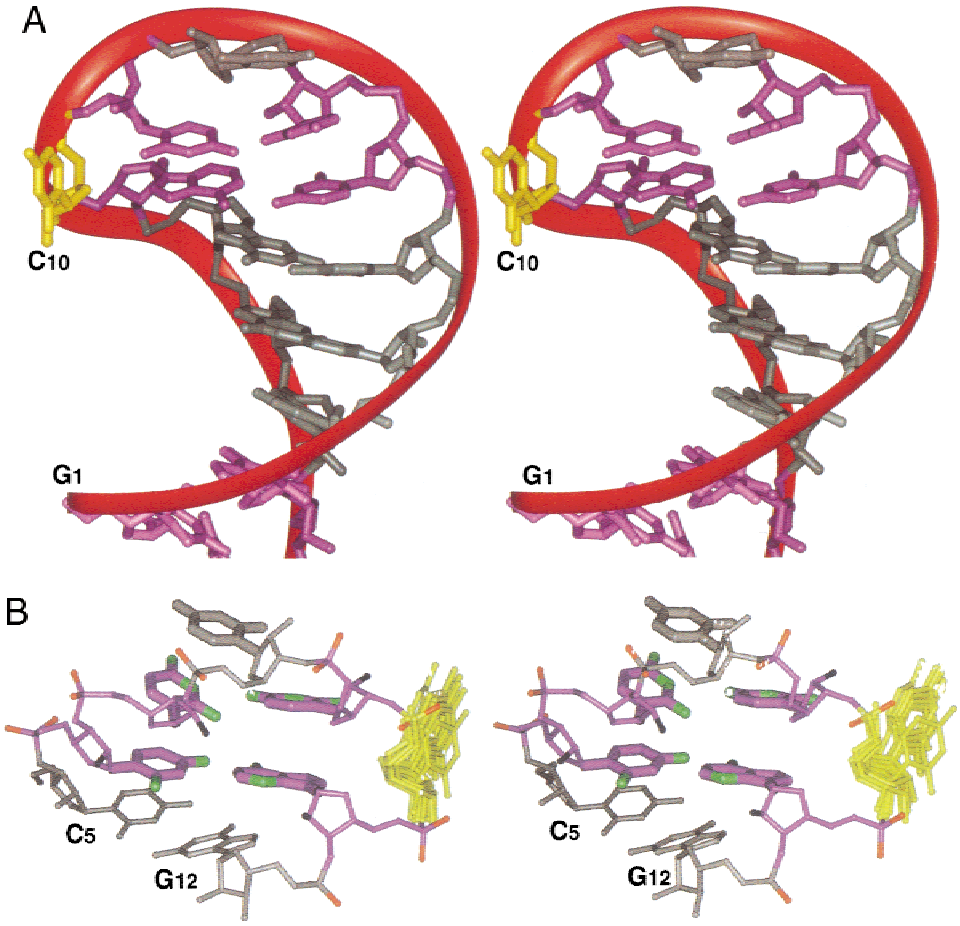

FIGURE 7. Stereoviews of the minimized average structure of the hairpin SL_{28} towards the major groove (**A**) and the loop and closing base pairs towards the minor groove (**B**). Nucleotides that are specifically required for SLBP binding are pink, conserved R and Y nucleotides are gray, and the variable loop nucleotide (C_{10}) is yellow. In the loop, functional groups of the conserved nucleotides available for hydrogen bond interactions with the SLBP are red: phosphoryl oxygen atoms; green: base nitrogen and oxygen atoms; and black: 2′ oxygen atoms. The sugar-phosphate backbone is not distorted in the stem region and the G_2•C_{15} base pair is not unusually positioned within the helix. In the loop, U_7 stacks on the U_6•A_{11} base pair and U_8 stacks on top of U_7. U_9 is positioned above A_{11} approximately coplanar with U_7 and points into the helix, but there is no evidence of hydrogen bonding between U_9 and U_7.

TABLE 2. C6, C8, and C1′ $T_{1\rho}$ relaxation times for the SL_{16} RNA molecule.

	$T_{1\rho}$ (ms)			$T_{1\rho}$ (ms)	
Residue	C6/8	C1′	Residue	C6/8	C1′
G_1	58	45	U_9	55	71
G_2	57	56	C_{10}	80	84
C_3	47	n.m.[a]	A_{11}	67	54
C_4	46	n.m.	G_{12}	54	68
C_5	48	n.m.	G_{13}	55	77
U_6	49	80	G_{14}	55	75
U_7	63	73	C_{15}	47	74
U_8	67	78	C_{16}	49	n.m.

The uncertainty in the measured relaxation times is ±5%.
[a]n.m.: not measured.

mary sequence requirements (Williams & Marzluff, 1995; Battle & Doudna, 2001) for binding. In addition, the large number of histone 3′ ends in the database allows one to deduce the functional consensus sequence from sequences in the database.

Structure of the RNA-binding site for histone SLBP

Despite many unusual non-A-form structural characteristics, the UUUC hairpin tetraloop has a very defined tertiary structure (Fig. 7). The 5′ base stack of the stem continues into the loop, with the U_7 base stacking on the U_6• A_{11} base pair in a normal A-form conformation, whereas the U_8 base stacks on U_7. The U_9 base stacks above A_{11} and the planes of the U_7 and U_9 bases are rotated ~25° to each other. The C_{10} base does not stack at all, but instead points out into solution parallel to the helix axis. Although the N3 of U_7 points toward the O4 of U_9 on the minor groove side of the helix (Fig. 7), there is no spectral evidence of hydrogen bonds between these bases. Thus, unless a network of water-mediated hydrogen bonds is organized within the loop, the preciseness of the structure calculations suggests that the loop may be effectively stabilized by stacking and hydrophobic interactions alone. The long $T_{1\rho}$ relaxation times of the C_{10} C6 and C1′ atoms and intermediate $T_{1\rho}$ relaxation times of the U_8 and U_9 C6 atoms (Table 2) indicate that these residues are mobile and may occupy a greater region of space than indicated by the structure calculations (Fig. 5A). However, the $T_{1\rho}$ relaxation times do not provide direct information on the amplitudes of the nucleotide motions, which may be small. Nevertheless, the conformational heterogeneity of C_{10} is consistent with the limited number of NOEs to its base.

The structure of the hairpin presented here is similar to that presented in the accompanying manuscript (Zanier et al., 2002). The stems are 6 bp in length, the third uridine of the loop stacks on the adenine of the loop-closing A•U base pair, and the loop cytidine extends out away from the helix. The conformational differences are localized to the stacking arrangement of the loop uridine residues (Fig. 7; Zanier et al., 2002, Fig. 5) and appear to be the result of the different buffer conditions. The greater ionic strength, more alkaline pH, and the use of K^+ as the counterion in this study appear to stabilize the 5′-stack of U_7 and U_8. The observation of the loop NH resonances in this study suggests that the conformation of the loop affords a greater degree of protection of the NH protons from solvent exchange. These conformational differences are likely due to small differences in the energy of these two possible states of the loop, and the actual structure of the loop in the cell is not known.

The conformations of the loops of both molecules are distinct from the structures of the unusually thermostable classes' tetraloops. The nucleotides at positions 1 and 4 of the pyrimidine-rich tetraloop motifs, UNCG and CUUG, form base pairs that enhance the thermodynamic stability of the RNA hairpin (Cheong et al., 1990; Jucker & Pardi, 1995). That guanine has been selected against in the fourth position of the loop of histone mRNA stem-loop sequences is consistent with the importance of a unique structure of the loop to histone mRNA metabolism.

The stem of the RNA hairpin contains six Watson–Crick base pairs and exhibits no evidence for unusual conformational deviations from canonical A-form geometry. Importantly, the experimental NOE and torsion angle constraints do not suggest backbone or intrahelical structure features unique to the G_2•C_{15}/C_3•G_{14} base pair junction that could serve as a specific recognition element for the histone SLBP (Fig. 7A). The apparent lack of helical deformation at this junction and the presentation of minor groove functional groups unique to G•C base pairs indicate these residues may form base-specific contacts to the histone SLBP.

The sequences flanking the stem do not adopt a unique secondary structure or tertiary fold. Indeed, this region does not even exhibit the propensity to form a stable secondary structure as revealed by the lack of protonation of A_{-3}, A_{-2}, A_{-1}, and A_{21} at an unusually high pH. The protonated form of adenine participates in the AH^+•C base pair (Legault & Pardi, 1994; Cai & Tinoco, 1996) and is made possible by an increase of the adenine pKa. The apparently normal pK_a values of the flanking sequence adenine bases combined with the long relaxation times of their C2 atoms support the very dynamic behavior of these residues.

Phylogenetic conservation of residues within the 3′ stem-loop structure

A previous prediction of the structure of the 3′ end of histone mRNA (Gabb et al., 1992) shows some simi-

larity to the structure we determined, with a 5′ stack on the stem and the fourth base of the loop flipped out. The stem is an A-form helix with no dramatic alterations from the canonical A-form geometry caused by the sequence. In the free RNA, there is no evidence for extensive ordering of the 5 nt 5′ to the stem, although these nucleotides make a large contribution to the overall binding affinity for SLBP (Williams & Marzluff, 1995). Thus it is likely that these nucleotides adopt a defined structure only after binding to the SLBP.

The mammalian histone mRNAs (over 100 different histone genes sequenced) have a very strong consensus in the stem-loop. The two G•C base pairs at the base of the stem are invariant and they are followed by Y•R base pairs, at least two of which are C•G base pairs, and the top base pair is U•A, which is also invariant. The first and third bases of the loop are always uridines, with the second base a pyrimidine in more than 95% of the genes. Detailed binding studies of the base pairs in the stem indicate that the second G•C base pair makes the largest single contribution to binding (Battle & Doudna, 2001), suggesting that there may be specific contacts between the RNA-binding domain (RBD) of SLBP and functional groups of the bases. Introduction of an additional base pair into the stem greatly reduced binding of SLBP to the stem-loop, suggesting that there may be precise orientation of the single-stranded 5′ flanking sequence with the base pairs near the base of the stem (Williams & Marzluff, 1995). Thus it is likely that the SLBP recognizes the stem-loop by recognizing the sequence of the stem, particularly the bottom base pairs and the pattern of pyrimidine–purine base pairs in the last 4 bp of the stem, and the 5′ stack of the loop. The variable fourth base, which is flipped out into the solvent, is unlikely to be an important contact for the SLBP. Because the variable fourth base of the loop is on the major groove face of the A-helix, we speculate that the SLBP binding site is on the other face, with the SLBP making specific contacts in the minor groove of the stem, as is the case for several other RNA-binding proteins (Draper, 1999). However, the structural data for the RNA alone does not allow us to exclude other binding mechanisms, such as induced fit, that lead to structural rearrangement of the loop nucleotides. The sequence and structure of the 3′ flanking region is not likely to be critical for high-affinity binding, because the SLBP binds both to the pre-mRNA and to the mature histone mRNA. The conservation of the sequence of the 3′ flanking region is necessary to specify the cleavage site and not as important for binding SLBP (Furger et al., 1998). The loop may also provide specific contacts for the SLBP; alternatively the substitutions of purines in positions 1 and 3 of the loop for the uridines may result in disruption of the overall geometry of the 5′ stack on the stem-loop, and thus interfere with RNA binding.

It is curious that there is a conserved U•A base pair at the top of stem. Most short stems are closed with a G•C base pair to impart extra stability to the structure. Thus we would not have been overly surprised if the actual structure of the stem-loop was a 5-bp stem and a 6-base loop. We have previously shown that converting the U•A base pair to a C•G base pair reduces binding affinity of SLBP and converting it to a U•G base pair was more deleterious, consistent with the base pair being present in the functional stem-loop structure (Williams & Marzluff, 1995). A functional correlation of changes in binding activity and histone mRNA expression showed an excellent agreement with these observations: there was 5–10-fold less mRNA expressed from the C•G stem-loop, less from the U•G stem loop and no detectable mRNA when the U•A base pair was changed to U•C (Pandey et al., 1994).

Role of the SLBP–stem-loop RNA complex

The stem-loop at the 3′ end of histone mRNA is involved in many of the functions of the histone mRNA. High-affinity binding of SLBP to the stem-loop is necessary for efficient 3′ processing of the histone mRNA (Dominski et al., 2001), so alterations in the stem-loop result in decreased synthesis of histone mRNA (Pandey et al., 1994). Other functions of the stem-loop include regulation of histone mRNA half-life (Pandey & Marzluff, 1987), and this may not be solely due to binding of SLBP. It is possible that the U•A base pair is involved in other functions of the stem-loop and it may be necessary, for example, to disrupt that base pair as part of the mechanism of histone mRNA degradation. This could account for the strong selection of the U•A base pair in the stem-loop structure.

There are few RNA-binding proteins that specifically recognize stem sequences of a stem-loop structure that is binding motif. More commonly the major specificity lies in the single-stranded region (Oubridge et al., 1994; Draper, 1999) or in a defect in the stem (Puglisi et al., 1992; Valegård et al., 1994). The SLBP has a novel RNA-binding domain, and there are no other proteins with a similar sequence to the SLBP RBD in the human, *Drosophila* (Sullivan et al., 2001) or *C. elegans* genomes (Martin et al., 2000). Thus it may be a unique RNA-binding protein that evolved as part of the regulatory mechanism for coordinately and precisely regulating the histone mRNA levels during the metazoan cell cycle. No similar proteins are present either in yeast or *Arabidopsis*, and the fungal and plant histone mRNAs all end in poly(A) tails. Because SLBP is the major *trans*-acting factor in regulation of histone mRNA in the mammalian cell cycle (Whitfield et al., 2000), understanding how this protein recognizes its RNA target will be very important to understanding how SLBP carries out the posttranscriptional regulation of histone mRNA function and metabolism.

MATERIALS AND METHODS

All enzymes were purchased from Sigma Chemical (St. Louis, Missouri) except for T7 RNA polymerase, which was prepared as described (Davanloo et al., 1984). Deoxyribonuclease I type II, pyruvate kinase, adenylate kinase, and nucleotide monophosphate kinase were obtained as powders, dissolved in 15% glycerol, 1 mM dithiothreitol, and 10 mM Tris-HCl, pH 7.4, and stored at −20 °C. Guanylate kinase and nuclease P1 were obtained as solutions and stored at −20 °C. Unlabeled 5′ nucleoside triphosphates (5′-NTPs) were purchased from Sigma, phosphoenolpyruvate (potassium salt) was purchased from Bachem, and 99% [^{15}N]-ammonium sulfate and 99% [^{13}C]-glucose were purchased from Cambridge Isotope Labs (Andover, Massachusetts).

Preparation of RNA samples

The RNA sequences depicted in Figure 1 were prepared by in vitro transcription with T7 RNA polymerase using a synthetic DNA template (Milligan et al., 1987) and either unlabeled or ^{15}N- and ^{13}C-labeled 5′-NTPs (Nikonowicz et al., 1992). To assist in the NMR assignment process, uniformly ^{13}C-enriched sample of the RNA molecules were prepared in which the pyrimidine C5 positions were deuterated (Nikonowicz et al., 1998). The RNA molecules were purified using 20% (w/v) preparative polyacrylamide gels, electroeluted (Schleicher & Schuell), and precipitated with ethanol. The purified RNA molecules were resuspended in 1.0 M NaCl, 20 mM KPi, pH 6.8, and 2.0 mM EDTA, and extensively dialyzed against 20 mM KCl, 20 mM KPi, pH 6.8, and 0.02 mM EDTA using a Centricon-3 concentrator (Millipore, Bedford, Massachusetts). All RNA samples were concentrated to a volume of 240 μL, lyophilized to a powder, and either resuspended in 90% H_2O/10% D_2O or exchanged twice with 99.9% D_2O and resuspended in 99.96% D_2O. The samples were then heated to 90 °C for 60 s and snap cooled on ice. The sample concentrations varied between 100 and 150 A_{260} O.D. in 240 μL (~2–3 mM).

NMR spectroscopy

All spectra were acquired on a Bruker, AMX-500 spectrometer equipped with ^{1}H-{^{13}C, ^{15}N} and ^{1}H-{^{13}C, ^{31}P} resonance probes. Solvent suppression for spectra collected in 90% H_2O was achieved using spin-lock pulses or binomial 1read pulses with maximum excitation at 12.5 ppm. Typically, the data points were extended by 25% using linear prediction for the indirectly detected dimensions and the data were apodized using 1 Hz line broadening and 65 degree shifted sinebell functions. NMR spectra were processed and analyzed using Felix 95.0 (Molecular Simulations, San Diego, California).

Two-dimensional ^{13}C-^{1}H HMQC and HSQC spectra were collected to identify ^{13}C-^{1}H chemical shift correlations for SL_{16} and SL_{28} RNAs. Sugar spin systems were assigned using three-dimensional HCCH-TOCSY (24 ms DIPSI-3 spin lock) experiments collected in D_2O. A two-dimensional HCCH-TOCSY (52 ms DIPSI-3 spin lock) was collected to establish the intrabase H2-C2-C8-H8 correlations in adenine residues in SL_{28} RNA. Two-dimensional ^{15}N-^{1}H HSQC experiments were acquired in D_2O and optimized for two- and three-bond couplings to identify intraresidue base-sugar correlations (Pardi, 1995; Dieckmann & Feigon, 1997).

Sequential assignments and distance constraints for the nonexchangeable resonances were derived at 25 °C from two-dimensional ^{1}H-^{1}H NOESY spectra (160, 250, and 350 ms mixing times) and three-dimensional ^{13}C-edited NOESY spectra (180, 280, and 400 ms mixing time) optimized for the ribose resonances in ω_2 and ω_3. For the exchangeable resonances, two-dimensional ^{15}N-^{1}H HSQC spectra were collected to identify ^{15}N-^{1}H chemical shift correlations. Two-dimensional ^{1}H-^{1}H NOESY spectra optimized for imino (NH) proton resonances in ω_2 were acquired at 250 and 400 ms mixing times in H_2O and at 7 °C to obtain distance restraints involving the exchangeable protons. A J(N, N)-HNN COSY experiment was acquired to confirm the presence of the U_6•A_{11} base pair (Hennig & Williamson, 2000).

$^{3}J_{H\text{-}H}$ coupling constants were determined from DQF-COSY experiments acquired in D_2O with ^{31}P decoupling. $^{3}J_{C\text{-}P}$ coupling constants were determined using the spin-echo difference method (Legault et al., 1995). $^{3}J_{P\text{-}H}$ couplings were measured using ^{31}P-^{1}H HetCor experiments.

^{13}C $T_{1\rho}$ relaxation times were measured using two-dimensional ^{13}C-^{1}H ctHSQC-based experiments (Yamazaki et al., 1994) optimized for C2, C6, C8, and C1′ resonances. A 2.3-kHz ^{13}C spin lock field was used with delays of 4, 8, 12, 20, 28, 36, 48, 68, and 96 ms. The 28-ms experiment was collected twice to provide an estimate of the error of the measured intensities. The ^{13}C-^{1}H cross peak volumes were fit to a single exponential decay.

Distance and torsion angle constraints

Interproton distance estimates were obtained from cross-peak intensities in two-dimensional NOESY and three-dimensional ^{13}C-edited NOESY spectra. Cross-peak intensities were calibrated using the pyrimidine H5-H6 fixed distance of 2.54 Å. NOE cross-peak intensities were classified as very strong, strong, medium, or weak and assigned upper distance bounds of 3.0, 4.0, 5.0, or 6.0 Å, respectively. Cross-peaks only observed in the longest mixing time spectra were classified as very weak and given an upper bound of 7.0 Å to accommodate the possibility of spin diffusion.

Base pairs were identified by downfield shifted NH or NH_2 proton resonances and by observation of strong G•C NH–NH_2 or A•U H2–NH NOEs. Hydrogen bonds were introduced as distance restraints of 2.9 ± 0.3 Å between donor and acceptor heavy atoms and 2.0 ± 0.2 Å between acceptor and hydrogen atoms. Constraints identified in this way were included in the calculations for the five G•C and one U•A base pairs of the stem.

Ribose ring pucker and backbone dihedral constraints were derived from $^{3}J_{H\text{-}H}$, $^{3}J_{H\text{-}P}$, and $^{3}J_{C\text{-}P}$ couplings (Varani et al., 1996). Ribose rings with $^{3}J_{H1'\text{-}H2'} > 7$ Hz and $^{3}J_{H3'\text{-}H4'} < 5$ Hz and with C3′ and C4′ resonances between 76 and 80 and 85 and 86 ppm, respectively, were constrained to the C2′-endo conformation. Residues with $^{3}J_{H1'\text{-}H2'} < 5$ Hz and large $^{3}J_{H3'\text{-}H4'} > 5$ Hz couplings were constrained to the C3′-endo conformation (Varani et al., 1996). Residues with intermediate $^{3}J_{H1'\text{-}H2'}$ couplings were left unconstrained. For residues in which H4′-H5′ and H4′-H5″ peaks in the DQF-COSY spectra were clearly absent, representing couplings <5 Hz, γ was constrained to the gauche$^+$ conformation (60 ± 20°). γ was left unconstrained for residues with clear $^{3}J_{H4'\text{-}H5'}$ or $^{3}J_{H4'\text{-}H5''} > 5$ Hz (indicating either the *trans* or gauche$^-$

conformation) or residues with weak $^3J_{H4'\text{-}H5'}$ or $^3J_{H4'\text{-}H5''}$, to reflect the possibility of conformational averaging (Varani et al., 1996). β was constrained to the *trans* conformation (180 $\pm$ 40°) for residues in which P-H5′ and P-H5″ peaks in the HetCor spectra were clearly absent, representing couplings $<$5 Hz. For residues in which P-H5′ and P-H5″ peaks could be observed, β was constrained to exclude the *trans* conformation. ϵ was constrained to exclude the gauche$^+$ conformation (-125 ± 105°) for residues with $^3J_{P\text{-}H3'} > 5$ Hz and $^3J_{P\text{-}C2'} < 5$ or $^3J_{P\text{-}C2'} > 5$ Hz (Varani et al., 1996). Dihedral angle restraints were not imposed for α and ζ.

Structure refinement

The dihedral angles of SL_{16} and SL_{28} model structures were randomized to generate 40 sets of coordinates for a simulated annealing/restrained molecular dynamics (rMD) routine using X-PLOR 3.851 (Brünger, 1992). The calculation protocol was divided into three stages: global fold, refinement, and final minimization. The first stage consisted of 10 ps of rMD at 1200 K using only ribose pucker, base pair, and NOE constraints, 15 ps of rMD at 1200 K during which repulsive van der Waals forces were introduced, 9 ps of rMD while cooling to 300 K, and minimized. Torsion angles β, γ, ϵ were introduced during an additional 5 ps of rMD at 1200 K while applying all other constraints and cooling to 300 K over 9 ps. The structures were then refined with 500 cycles of constrained minimization, 10 ps of rMD at 300 K using all constraints, and 1,000 cycles of constrained minimization. The final stage consisted of conjugate gradient energy minimization using all constraints and repulsive van der Waals potentials. The structures were analyzed using X-PLOR 3.851 and Insight II.

Note: Atomic coordinates for the refined structures have been deposited with the Protein Data Bank under accession code 1ju7 and 1jwc.

ACKNOWLEDGMENTS

We thank Malgorzata Michnicka for preparation of the T7 RNA polymerase and synthesis of the labeled 5′-nucleotide triphosphates, Dr. S. Moran for acquisition of the HNN-COSY experiment, and Dr. F. Haberle of Bruker Institute for providing access to the ^{1}H-{^{13}C, ^{31}P} triple resonance probe. This work was supported by Welch Foundation grant C1277 to E.P.N. and by National Institutes of Health Grant GM29832 to W.F.M. E.S.D. was supported by National Institutes of Health Predoctoral Training Grant GM08280.

Received August 17, 2001; returned for revision September 27, 2001; revised manuscript received October 17, 2001

REFERENCES

Battle DJ, Doudna JA. 2001. The stem-loop binding protein forms a highly stable and specific complex with the 3′ stem-loop of histone mRNAs. *RNA 7*:123–132.

Birnstiel ML, Busslinger M, Strub K. 1985. Transcription termination and 3′ processing: The end is in site! *Cell 41*:349–359.

Brünger AT. 1992. *X-PLOR Version 3.1 Manual*, New Haven, Connecticut: Yale University.

Cai Z, Tinoco IJ. 1996. Solution structure of loop A from the hairpin ribozyme from tobacco ringspot virus satellite. *Biochemistry 35*: 6026–6036.

Cheong C, Varani G, Tinoco I Jr. 1990. Solution structure of an unusually stable RNA hairpin, 5′GGAC(UUCG)GUCC. *Nature 346*: 613–614.

Davanloo P, Rosenburg AH, Dunn JJ, Studier FW. 1984. Cloning and expression of the gene for bacteriophage T7 RNA polymerase. *Proc Natl Acad Sci USA 81*:2035–2039.

Dieckmann T, Feigon J. 1996. Assignment methodology for larger RNA oligonucleotides: Application to an ATP-binding RNA aptamer. *J Biomol NMR 9*:259–272.

Dominski Z, Erkmann JA, Greenland JA, Marzluff WF. 2001. Mutations in the RNA binding domain of stem-loop binding protein define separable requirements for RNA binding and histone pre-mRNA processing. *Mol Cell Biol 21*:2008–2017.

Dominski Z, Marzluff WF. 1999. Formation of the 3′ end of histone mRNA. *Gene 239*:1–14.

Dominski Z, Zheng L-X, Sanchez R, Marzluff WF. 1999. The stem-loop binding protein facilitates 3′ end formation by stabilizing U7 snRNP binding to the histone pre-mRNA. *Mol Cell Biol 19*:3561–3570.

Draper DE. 1999. Themes in RNA-protein recognition. *J Mol Biol 293*:255–270.

Eckner R, Ellmeier W, Birnstiel ML. 1991. Mature mRNA 3′ end formation stimulates RNA export from the nucleus. *EMBO J 10*: 3513–3522.

Furger A, Schaller A, Schümperli D. 1998. Functional importance of conserved nucleotides at the histone RNA 3′ processing site. *RNA 4*:246–256.

Gabb HA, Harris ME, Pandey NB, Marzluff WF, Harvey SC. 1992. Molecular modeling to predict the structural and biological effects of mutations in a highly conserved histone mRNA loop sequence. *J Biomol Struc Dynamics 9*:1119–1131.

Gick O, Krämer A, Keller W, Birnstiel ML. 1986. Generation of histone mRNA 3′ ends by endonucleolytic cleavage of the pre-mRNA in a snRNP-dependent in vitro reaction. *EMBO J 5*:1319–1326.

Gick O, Krämer A, Vasserot A, Birnstiel ML. 1987. Heat-labile regulatory factor is required for 3′ processing of histone precursor mRNAs. *Proc Natl Acad Sci USA 84*:8937–8940.

Gorenstein DG. 1984. *Phosphorus-31 NMR: Principles and Applications*, New York: Academic Press.

Hennig M, Williamson JR. 2000. Detection of N-H•••N hydrogen bonding in RNA via scalar couplings in the absence of observable imino proton resonances. *Nucleic Acids Res 28*:1585–1593.

Jucker FM, Pardi A. 1995. Solution structure of the CUUG hairpin loop: A novel RNA tetraloop motif. *Biochemistry 34*:14416–14427.

Legault P, Jucker FM, Pardi A. 1995. Improved measurement of ^{13}C, ^{31}P J coupling constants in isotopically labeled RNA. *FEBS Lett 362*:156–160.

Legault P, Pardi A. 1994. In situ probing of adenine protonation in RNA by ^{13}C NMR. *J Am Chem Soc 116*:8390–8391.

Lüscher B, Schümperli D. 1987. RNA 3′ processing regulates histone mRNA levels in a mammalian cell mutant. A processing factor becomes limiting in G1-arrested cells. *EMBO J 6*:1721–1726.

Martin F, Michel F, Zenklusen D, Müller B, Schümperli D. 2000. Positive and negative mutant selection in the human histone hairpin-binding protein using the yeast three-hybrid system. *Nucleic Acids Res 28*:1594–1603.

Martin F, Schaller A, Eglite S, Schümperli D, Müller B. 1997. The gene for histone RNA hairpin binding protein is located on human chromosome 4 and encodes a novel type of RNA binding protein. *EMBO J 16*:769–778.

Marzluff WF. 1992. Histone 3′ ends: Essential and regulatory functions. *Gene Expr 2*:93–97.

Milligan JF, Groebe DR, Witherell GW, Uhlenbeck OC. 1987. Oligoribonucleotide synthesis using T7 RNA polymerase and synthetic DNA templates. *Nucleic Acids Res 15*:8783–8789.

Mowry KL, Steitz JA. 1987. Identification of the human U7 snRNP as one of several factors involved in the 3′ end maturation of histone premessenger RNA's. *Science 238*:1682–1687.

Nikonowicz EP, Michnicka M, DeJong E. 1998. Improved NOE-based sequential correlation of base-1′ proton resonances in labeled nucleic acids. *J Am Chem Soc 120*:3813–3814.

Nikonowicz EP, Sirr A, Legault P, Jucker FM, Baer LM, Pardi A. 1992. Preparation of ^{13}C and ^{15}N labelled RNAs for heteronuclear multidimensional NMR studies. *Nucleic Acids Res 20*:4507–4513.

Oubridge C, Ito N, Evans PR, Teo C-H, Nagai K. 1994. Crystal structure at 1.92 Å resolution of the RNA binding domain of the U1A spliceosomal protein complexed with an RNA hairpin. *Nature 372*:432–438.

Pandey NB, Marzluff WF. 1987. The stem-loop structure at the 3′ end of histone mRNA is necessary and sufficient for regulation of histone mRNA stability. *Mol Cell Biol 7*:4557–4559.

Pandey NB, Williams AS, Sun J-H, Brown VD, Bond U, Marzluff WF. 1994. Point mutations in the stem-loop at the 3′ end of mouse histone mRNA reduce expression by reducing the efficiency of 3′ end formation. *Mol Cell Biol 14*:1709–1720.

Pardi A. 1995. Multidimensional heteronuclear NMR experiments for structure determination of isotopically labeled RNA. *Methods Enzymol 261*:350–380.

Puglisi JD, Tan R, Calnan BJ, Frankel AD, Williamson JR. 1992. Conformation of the TAR RNA-arginine complex by NMR spectroscopy. *Science 257*:76–80.

Roberts SB, Emmons SW, Childs G. 1989. Nucleotide sequences of *Caenorhabditis elegans* core histone genes. Genes for different histone classes share common flanking sequence elements. *J Mol Biol 206*:567–577.

Soldati D, Schümperli D. 1988. Structural and functional characterization of mouse U7 small nuclear RNA active in 3′ processing of histone pre-mRNA. *Mol Cell Biol 8*:1518–1524.

Sullivan E, Santiago C, Parker ED, Dominski Z, Yang X, Lanzotti DJ, Ingledue TC, Marzluff WF, Duronio RJ. 2001. *Drosophila* stem loop binding protein coordinates accumulation of mature histone mRNA with cell cycle progression. *Genes & Dev 15*:173–187.

Valegård K, Murray JB, Stockley PG, Stonehouse NJ, Liljas L. 1994. Crystal structure of an RNA bacteriophage coat protein-operator complex. *Nature 371*:623–626.

Varani G, Aboul-ela F, Allain FH-T. 1996. NMR investigation of RNA structure. *Prog Nucleic Magn Reson Spectrosc 29*:51–127.

Wang Z-F, Whitfield ML, Ingledue TI, Dominski Z, Marzluff WF. 1996. The protein which binds the 3′ end of histone mRNA: A novel RNA-binding protein required for histone pre-mRNA processing. *Genes & Dev 10*:3028–3040.

Whitfield ML, Zheng L-X, Baldwin A, Ohta T, Hurt MM, Marzluff WF. 2000. Stem-loop binding protein, the protein that binds the 3′ end of histone mRNA, is cell cycle regulated by both translational and posttranslational mechanisms. *Mol Cell Biol 20*:4188–4198.

Williams AS, Ingledue TC, Kay BK, Marzluff WF. 1994. Changes in the stem-loop at the 3′ terminus of histone mRNA affects its nucleocytoplasmic transport and cytoplasmic regulation. *Nucleic Acids Res 22*:4660–4666.

Williams AS, Marzluff WF. 1995. The sequence of the stem and flanking sequences at the 3′ end of histone mRNA are critical determinants for the binding of the stem-loop binding protein. *Nucleic Acids Res 23*:654–662.

Yamazaki T, Muhandiram R, Kay LE. 1994. NMR experiments for the measurement of carbon relaxation properties in highly enriched, uniformly ^{13}C, ^{15}N-labeled proteins: Application to $^{13}C^{\alpha}$ carbons. *J Am Chem Soc 116*:8266–8278.

Zanier K, Luten I, Crombie C, Müller B, Schümperli D, Linge JP, Nilges M, Sattler M. 2002. Structure of the histone mRNA hairpin required for cell cycle regulation of histone gene expression. *RNA 8*:29–46.

APPENDIX

Tables A1–A4 list the chemical shifts of the ^{1}H, ^{13}C, and ^{15}N resonances.

TABLE A1. Chemical shifts (in parts per million) of the proton resonances of the SL_{28} RNA.

Res.	H1′	H2″	H3′	H4′	H5′/H5″	H6/H8	H5	H2	NH_2	NH
G_{-7}	5.88	na	na	na	na	7.99			na	na
G_{-6}	5.83	na	na	na	na	7.43			na	na
C_{-5}	5.56	na	na	na	na	7.64	5.27		na	
C_{-4}	na	na	na	na	na	na	na		na	
A_{-3}	5.82	na	na	na	na	7.92		7.06	na	
A_{-2}	5.51	na	na	na	na	7.85		7.83	na	
A_{-1}	6.01	na	na	na	na	8.17		8.14	na	
G_1	5.92	4.99	4.78	4.54	4.43/4.22	8.01			na	11.90
G_2	5.94	4.61	4.63	4.59	4.55/4.33	7.55			na	13.11
C_3	5.62	4.47	4.50	4.48	4.59/4.14	7.73	5.33		8.82/7.02	
C_4	5.55	4.46	4.48	4.45	4.57/4.11	7.81	5.60		8.69/7.01	
C_5	5.54	4.43	4.47	4.43	4.60/4.09	7.81	5.54		8.57/6.97	
U_6	5.76	4.46	4.53	4.41	4.50/4.08	7.72	5.48			13.68
U_7	5.57	4.25	4.44	4.35	4.23/4.06	7.77	5.78			na
U_8	5.90	4.39	4.48	4.37	4.09/3.99	7.76	5.88			na
U_9	5.55	4.18	4.52	3.98	3.96/3.93	7.36	5.72			10.48
C_{10}	6.06	4.47	4.61	4.59	4.29/4.14	7.88	6.00		7.16/6.70	
A_{11}	6.00	4.82	4.68	4.61	4.45/4.28	8.37		7.63	na	
G_{12}	5.75	4.61	4.53	4.50	4.52/4.17	7.42			8.50/7.17	12.57
G_{13}	5.83	4.62	4.57	4.53	4.50/4.09	7.25			8.70/7.03	12.57
G_{14}	5.82	4.03	4.22	4.17	4.53/4.06	7.26			8.58/7.01	13.03
C_{15}	5.80	4.56	4.51	4.53	4.51/4.08	7.67	5.29		8.75/7.10	
C_{16}	5.51	4.39	4.50	4.41	4.50/4.11	7.65	5.51		8.60/7.23	
A_{17}	5.88	na	na	na	na	7.92		7.19	na	
C_{18}	5.07	na	na	na	na	7.19	5.19		na	
C_{19}	5.52	na	na	na	na	7.60	5.51		na	
C_{20}	5.72	na	na	na	na	7.67	5.61		na	
A_{21}	6.07	na	na	na	na	8.45		8.20	na	

The nonexchangeable ^{1}H chemical shifts were measured at 25 °C and pH 6.8 and are referenced to the residual ^{2}HOH resonance at 4.76 ppm. Exchangeable proton chemical shifts were measured at 12° and referenced to the H_2O resonance at 4.89 ppm. The uncertainties in the chemical shift values are ~0.02 ppm. The 5′ and 5″ protons are not stereospecifically assigned.

na: not available.

TABLE A2. Chemical shifts (in parts per million) of the carbon and nitrogen resonances of the SL_{28} RNA.

Atom	C1′	C2′	C3′	C4′	C5′	C6/C8	C5	C2	N1/N9	N1/N3	N1/N3	N2/N4/N6
G_{-7}	93.13	na	na	na	na	138.34			na	na		na
G_{-6}	92.94	na	na	na	na	136.66			na	na		na
C_{-5}	92.56	na	na	na	na	na	na		na			na
C_{-4}	na	na	na	na	na	na	na		na			na
A_{-3}	93.22	na	na	na	na	139.88		153.71	na		na	na
A_{-2}	92.14	na	na	na	na	139.97		154.99	na		na	na
A_{-1}	90.22	na	na	na	na	141.32		155.61	na		na	na
G_1	93.13	75.29	75.3	83.9	67.4	139.03			165.21	145.37		na
G_2	92.84	75.55	73.2	82.8	66.5	137.24			166.62	145.70		na
C_3	94.12	75.80	72.4	82.2	64.9	141.14	97.30		187.90			96.34
C_4	94.49	75.53	72.5	82.2	65.0	141.48	98.58		187.77			95.52
C_5	94.48	75.66	72.4	82.2	64.9	141.36	98.13		187.90			95.52
U_6	92.63	75.87	73.9	83.4	65.4	141.95	104.15		183.20	158.95		
U_7	93.12	75.51	75.5	84.5	67.0	143.10	105.14		181.50	155.01		
U_8	89.52	75.35	78.1	86.2	68.0	143.62	105.80		179.55	154.96		
U_9	90.14	76.28	77.5	85.4	68.1	142.97	105.60		180.27	154.79		
C_{10}	91.26	76.22	76.8	84.6	67.9	143.53	99.52		187.09			91.76
A_{11}	93.12	75.74	74.5	83.2	67.2	140.86		153.63	167.73		174.45/166.79	na
G_{12}	92.75	75.77	73.2	82.3	66.2	136.76			167.24	144.41		84.70
G_{13}	93.01	75.73	73.1	82.9	65.7	136.49			166.67	145.01		84.63
G_{14}	93.12	77.82	69.8	83.5	65.3	136.45			166.24	146.00		84.58
C_{15}	93.95	75.70	72.2	82.9	64.8	141.07	98.561		187.81			96.44
C_{16}	93.37	75.39	73.0	82.6	65.6	141.62	99.45		189.32			na
A_{17}	93.03	na	na	na	na	139.32		154.18	na		na	na
C_{18}	93.50	na	na	na	na	140.35	na		na			na
C_{19}	94.15	na	na	na	na	na	na		na			na
C_{20}	92.75	na	na	na	na	143.43	na		na			na
A_{21}	90.94	na	na	na	na	142.15		155.87	na		na	na

The ^{15}N chemical shifts are reported relative to an external standard of NH_4OH and were recorded at 12 °C and pH 6.8. The ^{13}C chemical shifts are reported relative to an external standard of TSP and were recorded at 25 °C. The chemical shifts have uncertainties of ~0.05 and ~0.03 ppm for ^{13}C and ^{15}N, respectively. The 3′, 4′, and 5′ ^{13}C resonance chemical shifts have been rounded to the nearest 0.1 ppm to reflect the added uncertainty in identifying the cross-peak centers due to spectral congestion.

na: not available.

TABLE A3. Chemical shifts (in parts per million) of the proton resonances of the SL_{16} RNA.

Atom	H1′	H2″	H3′	H4′	H5′/H5″	H6/H8	H5	H2	NH_2	NH
G_1	5.85	4.97	4.79	4.59	4.41/4.30	8.17			na	12.85
G_2	5.96	4.60	4.62	4.59	4.55/4.35	7.65			na	13.44
C_3	5.62	4.47	4.50	4.49	4.59/4.14	7.76	5.33		8.80/7.02	
C_4	5.55	4.46	4.48	4.45	4.57/4.11	7.80	5.59		8.69/7.01	
C_5	5.54	4.40	4.49	4.43	4.58/4.10	7.81	5.54		8.57/6.99	
U_6	5.76	4.48	4.53	4.40	4.50/4.09	7.71	5.48			13.68
U_7	5.55	4.25	4.46	4.34	4.24/4.03	7.77	5.79			na
U_8	5.90	4.39	4.48	4.38	4.08/3.99	7.78	5.88			na
U_9	5.55	4.18	4.52	3.99	3.97/3.92	7.36	5.73			10.48
C_{10}	6.08	4.47	4.59	4.60	4.27/4.15	7.88	6.00		7.16/6.70	
A_{11}	6.00	4.81	4.66	4.61	4.44/4.29	8.37		7.63	na	
G_{12}	5.75	4.63	4.52	4.50	4.52/4.18	7.42			8.50/7.17	12.57
G_{13}	5.84	4.66	4.53	4.52	4.53/4.11	7.25			8.70/7.03	12.57
G_{14}	5.82	4.05	4.20	4.19	4.53/4.06	7.26			8.58/7.01	13.08
C_{15}	5.82	4.57	4.50	4.51	4.52/4.08	7.67	5.26		8.77/7.07	
C_{16}	5.59	4.36	4.46	4.44	4.58/4.07	7.73	5.61		8.50/7.15	

The nonexchangeable ^1H chemical shifts were measured at 25 °C and pH 6.8 and are referenced to the residual ^2HOH resonance at 4.76 ppm. Exchangeable proton chemical shifts were measured at 12° and referenced to the H_2O resonance at 4.89 ppm. The uncertainties in the chemical shift values are ~0.02 ppm. The 5′ and 5″ protons are not stereospecifically assigned.

na: not available.

TABLE A4. Chemical shifts (in parts per million) of the carbon and nitrogen resonances of the SL_{16} RNA.

Atom	C1′	C2′	C3′	C4′	C5′	C6/C8	C5	C2	N1/N9	N1/N3	N1/N3	N2/N4/N6
G_1	91.76	75.19	75.27	83.97	67.43	139.34			165.24	145.15		na
G_2	93.24	75.58	73.17	82.80	66.49	137.44			166.63	145.75		na
C_3	94.12	75.81	72.40	82.18	64.86	141.14	97.32		187.90			96.39
C_4	94.49	75.50	72.47	82.18	65.02	141.48	98.59		187.75			95.52
C_5	94.49	75.66	72.40	82.18	64.86	141.36	98.13		187.90			95.52
U_6	93.12	75.89	73.87	83.42	65.41	141.95	104.17		183.20	158.96		
U_7	92.63	75.50	75.50	84.51	66.96	143.10	105.14		181.50	155.01		
U_8	89.52	75.35	78.07	86.22	67.97	143.62	105.84		179.57	154.93		
U_9	90.14	76.28	77.52	85.36	68.12	142.97	105.55		180.27	154.79		
C_{10}	91.26	76.20	76.82	84.59	67.97	143.56	99.45		187.13			91.76
A_{11}	93.12	75.74	74.49	83.19	67.19	140.86		153.63	167.71		174.45/166.79	na
G_{12}	92.75	75.74	73.25	82.26	66.18	136.76			167.24	144.41		84.73
G_{13}	93.00	75.73	73.09	82.18	65.72	136.45			166.63	145.01		84.63
G_{14}	93.12	77.83	69.83	83.50	65.33	136.45			166.24	146.03		84.63
C_{15}	94.49	75.74	72.24	82.18	64.79	141.11	98.59		187.90			96.39
C_{16}	93.25	75.50	73.02	82.64	65.64	141.76	99.45		189.36			na

The ^{15}N chemical shifts are reported relative to an external standard of NH_4OH and were recorded at 12 °C and pH 6.8. The ^{13}C chemical shifts are reported relative to an external standard of TSP and were recorded at 25 °C. The chemical shifts have uncertainties of ~0.05 and ~0.03 ppm for ^{13}C and ^{15}N, respectively.

na: not applicable.